(22 deg^2) and ribonuclease A (24 deg^2), and the average translation in papain (0·14 Å^2) is similar to that for ribonuclease A (0·11 Å^2).

For the solvent-accessible residues, the average libration is considerably greater for ribonuclease A (97 deg^2) than for papain (57 deg^2), whereas the average translation is greater for papain (0·23 Å^2) than for ribonuclease A (0·14 Å^2). The mean librations appear similar for the buried residues in both proteins as might be expected from the close-packed nature of these residues. The mean librations are greater for the solvent-accessible residues in ribonuclease A than for those in papain and thus the larger average librations found in ribonuclease A are accounted for by the greater percentage of surface groups having higher librations.

The mean translations are generally higher in papain than in ribonuclease A, especially the solvent-accessible residues. Thus there is more motion in papain of a translational nature, whereas for ribonuclease A, the motion is comprised in the main of surface-group librations.

Some of the motions described here may be of biological significance. For instance, in papain His 159 rocks about a single conformation; this may be of importance for catalysis because the histidine is expected to rock to protonate the proposed tetrahedral intermediate. His 119 in ribonuclease occupies two positions and multiple positions may be important for catalysis by this enzyme.

References

CRUICKSHANK, D. W. J. (1957). *Acta Cryst.* **10**, 504–508.

DRIESSEN, H. P., HANEEF, M. I. J., HARRIS, G. W., HOWLIN, B., KHAN, G. & MOSS, D. S. (1989). *J. Appl. Cryst.* **22**, 510–516.

GLOVER, I. D., MOSS, D. S., TICKLE, I. J., PITTS, J. E., HANEEF, I., WOOD, S. P. & BLUNDELL, T. L. (1985). *Adv. Biophys.* **20**, 1–12.

HANEEF, I., MOSS, D. S., STANFORD, M. J. & BORKAKOTI, N. (1985). *Acta Cryst.* A**41**, 426–433.

HARRIS, G. W. & MOSS, D. S. (1992). *Acta Cryst.* A**48**, 42–45.

HOLBROOK, S. R., DICKERSON, R. E. & KIM, S. H. (1985). *Acta Cryst.* B**41**, 255–262.

HOLBROCK, S. R. & KIM, S. H. (1984). *J. Mol. Biol.* **173**, 361–388.

HOLBROOK, S. R., WANG, A. H. J., RICH, A. & KIM, S. H. (1986). *J. Mol. Biol.* **187**, 429–440.

HOWLIN, B. & DRIESSEN, H. (1986). *TLSANL*. Unpublished computer program.

HOWLIN, B., MOSS, D. S. & HARRIS, G. W. (1989). *Acta Cryst.* A**45**, 851–861.

JOHNSON, C. K. (1965). *ORTEP*. Report ORNL-3794. Oak Ridge National Laboratory, Tennessee, USA.

JOHNSON, C. K. & LEVY, H. A. (1974). *International Tables for X-ray Crystallography*, Vol. IV, edited by J. A. IBERS & W. C. HAMILTON, pp. 320–322. Birmingham: Kynoch Press. (Present distributor Kluwer Academic Publishers, Dordrecht.)

LEE, B. & RICHARDS, F. M. (1971). *J. Mol. Biol.* **55**, 379–400.

PICKERSGILL, R. W., HARRIS, G. W. & GARMAN, E. (1992). *Acta Cryst.* B**48**, 59–67.

SALI, A., VEERAPANDIAN, B., COOPER, J. B., MOSS, D. S., HOFMANN, T. & BLUNDELL, T. L. (1990). *J. Mol. Biol.* In the press.

SCHOMAKER, V. & TRUEBLOOD, K. N. (1968). *Acta Cryst.* B**24**, 63–76.

Acta Cryst. (1992). B**48**, 75–88

Structure Determination of Monoclinic Canine Parvovirus

BY JUN TSAO,* MICHAEL S. CHAPMAN, HAO WU, MAVIS AGBANDJE, WALTER KELLER AND MICHAEL G. ROSSMANN

Department of Biological Sciences, Purdue University, West Lafayette, Indiana 47907, *USA*

(*Received* 30 *April* 1991; *accepted* 2 *August* 1991)

Abstract

The three-dimensional structure of the single-stranded DNA canine parvovirus has been determined to 3.25 Å resolution. Monoclinic crystals belonging to space group $P2_1$ (a = 263.1, b = 348.9, c = 267.2 Å, β = 90.82°) were selected for data collection using primarily the Cornell High Energy Synchrotron Source and oscillation photography. There was one icosahedral particle per crystallographic asymmetric unit, giving 60-fold redundancy. The particle orientations in the unit cell were determined with a rotation function. The rough positions of the particles in the unit cell were estimated by considering the packing of spheres into the $P2_1$ crystal cell. More accurate particle centers were determined from Harker peaks in a Patterson function. Hollow-shell models were used to compute phases to 20 Å resolution. The radii of the models were based on packing considerations, the fit of spherical shells to the low-resolution X-ray data and

* Present address: Department of Microbiology, Center for Macromolecular Crystallography, University of Alabama, Birmingham, Alabama 35294, USA.

0108-7681/92/010075-14$03.00

low-angle solution scattering data. The phases were extended to 9 Å resolution using molecular replacement real-space averaging. These were then used to determine the heavy-atom position of a K_2PtBr_6 derivative, for which only 5% of the theoretically observable reflections had been recorded. The center of gravity of the 60 independent heavy-atom sites gave an improved particle center position. Single isomorphous replacement phases to 8 Å resolution were then calculated with the platinum derivative. These were used to initiate phase improvement and extension to 3.25 Å resolution using density averaging and Fourier back-transformation in steps of one reciprocal lattice point at a time. The resulting electron density map was readily interpretable and an atomic model was built into the electron density map on a PS390 graphics system using the *FRODO* program. The *R* factor prior to structure refinement for data between 5.0 and 3.25 Å was 36%.

Introduction

Canine parvovirus (CPV), the newest member of the autonomous replicating parvovirus family (Tattersall & Gardiner, 1990; Tattersall & Cotmore, 1990), was first identified in 1978 (Parrish, Have, Foreyt, Evermann, Senda & Carmichael, 1988) and has now infected almost every population of domestic and wild dogs. Autonomous parvoviruses infect and then destroy highly proliferating cells. Consequently, they can cause fatal disease in young or unborn mammals. CPV infections of dogs between 2 to 4 months of age can cause panleukopenia (*i.e.* all types of white blood cells are destroyed). Young dogs may develop myocarditis and die due to heart failure (Studdert, 1990). Parvoviruses can infect dogs, cats, rodents, humans and other mammals. The human parvovirus B19 is the cause of acute episodes of bone marrow failure (Kurtzman, Frickhofen, Kimball, Jenkins, Nienhuis & Young, 1989).

The CPV virion has a non-enveloped protein coat containing a linear single-stranded DNA molecule which is complementary to the coding sense. Electron micrographs showed the particle has a spherical shape, approximately 260 Å in diameter (Tattersall & Gardiner, 1990). The molecular weight of the infectious virion is about 5.5 to 6.2×10^6 daltons, of which 1.6×10^6 daltons is DNA. There are three types of capsid proteins, designated VP-1, VP-2 and VP-3 with molecular weights of 83000, 67300 and 63500 daltons, respectively (Paradiso, Rhode & Singer, 1982). VP-1 and VP-2 are transcribed from the same open reading frame, but the initiation site of VP-2 is downstream from that of VP-1. VP-3 is a post-translational modification product of VP-2 in which 15 to 18 amino-acid residues have been removed from the amino end. VP-1, VP-2 and VP-3 all exist in the infectious virion which contains a total of 60 protein subunits with VP-2 predominating.

The structure determination of viruses is heavily dependent on the use of noncrystallographic symmetry to refine and extend phasing to higher resolution (Rossmann, 1990). Initial phases to relatively low resolution have been obtained from isomorphous replacement data [*e.g.* human rhinovirus 14 (Rossmann, Arnold, Erickson, Frankenberger, Griffith, Hecht, Johnson, Kamer, Luo, Mosser, Rueckert, Sherry & Vriend, 1985), poliovirus (Hogle, Chow & Filman, 1985) and black beetle virus (Hosur, Schmidt, Tucker, Johnson, Gallagher, Selling & Rueckert, 1987)]. Surveys for heavy-atom derivatives and subsequent data collection are both time consuming and require many more crystals. These problems can be avoided by using an atomic model to obtain initial phases [*e.g.* Mengo virus (Luo, Vriend, Kamer, Minor, Arnold, Rossmann, Boege, Scraba, Duke & Palmenberg, 1987), human rhinovirus 1A (Kim, Smith, Chapman, Rossmann, Pevear, Dutko, Felock, Diana & McKinlay, 1989) and foot-and-mouth disease virus (Acharya, Fry, Stuart, Fox, Rowlands & Brown, 1989)]. However, there was no known structure of a related virus to provide initial phases for CPV. In some early examples, phases had been initiated not from an atomic model but from essentially spherical models [southern bean mosaic virus (Johnson, Akimoto, Suck, Rayment & Rossmann, 1976) and polyoma virus (Rayment, Baker, Caspar & Murakami, 1982)], but phase extension had not been continued beyond about 20 Å resolution. Here we report phasing which was initiated with a 20 Å resolution spherical model. These phases were then used to determine heavy-atom sites of a derivative for which only 5% of the data had been collected. The high-resolution structure was then determined starting from 8 Å resolution single isomorphous replacement (SIR) phases. With hindsight, we show here that it would have been possible to solve the structure without the use of the derivative.

Crystal preparation and data handling

The virus was propagated and purified by the modified procedure of Paradiso (1981) as described by Luo, Tsao, Rossmann, Basak & Compans (1988) and Tsao, Chapman, Agbandje, Keller, Smith, Wu, Luo, Smith, Rossmann, Compans & Parrish (1991). The final purification step was to centrifuge the virus through a CsCl gradient ($\rho = 1.4$ g cm^{-3}) for 20 h at 36000 rev min^{-1} in a Beckman SW41 rotor. In general, there were two bands with an A_{260}/A_{280} ratio of 0.70 for the top band and 1.43 for the bottom band.

Electron microscopy of negatively stained particles showed that these bands corresponded to empty and full virions. Useful crystals were obtained for both full and empty particles using 0.75% PEG 8000, 6 m*M* $CaCl_2$ in 10 m*M* Tris.HCl buffer at pH 7.5 in the reservoir, over which was suspended a hanging drop of 5 μl of virus solution diluted by 5 μl of the reservoir solution. Unfortunately, the crystals came out in a variety of forms of which the monoclinic (Luo *et al.*, 1988) and tetragonal (H. Wu, W. Keller & M. Agbandje, unpublished results) were the most usual. We report here the structure determination of the monoclinic crystal form. The cell dimensions are $a = 263.1$, $b = 348.9$, $c = 267.2$ Å, $\beta = 90.82°$ with space group $P2_1$ and one virion per asymmetric unit. Data collection was performed primarily at the Cornell High Energy Synchrotron Source (CHESS), although some data were collected at synchrotrons in Daresbury (England), Hamburg (Germany) and Brookhaven (New York). No attempt was made to orient the crystals in order to avoid radiation damage incurred during crystal setting and because the crystals lacked clear morphology. At CHESS, where the wavelength was 1.56 Å, a crystal-to-film distance of 100 mm was used. Oscillation angles of 0.4 to 0.7° were employed, with the majority of films taken with a 0.4° oscillation range. The crystals were maintained at 277 K during X-ray exposure. Three to six useful films could be obtained from one crystal. A special effort was made to collect very low-resolution data in order to help with the *ab initio* phasing using a spherical model. For this purpose, a 300 mm crystal-to-film distance was used together with a helium path and an oscillation angle of 2°. Among 253 films, about 30 films were collected with the large crystal-to-film distance.

Initial indexing was obtained primarily by using Kim's auto-indexing procedure (Kim, 1989). The program *INTEX* was used for more difficult films (M. S. Chapman, unpublished), which works according to the same principle as Kim's procedure, but substitutes adjustments through interactive graphics for automatic pattern recognition. The data were then processed and post-refined using the Purdue film processing package (Rossmann, 1979; Rossmann, Leslie, Abdel-Meguid & Tsukihara, 1979). Where there were partial reflections from films of abutting oscillation ranges, reflections were added to determine the full intensity. Reflections with a partiality greater than 0.5, for which there were no abutting film data, were also included, after correction, in the data set.

An essentially complete data set was collected for infectious particles containing a full complement of DNA (Table 1). Some data were also collected for empty capsids isomorphous with the full particle crystals. In addition, small amounts of data were collected for three heavy-atom derivatives (Table 1). Three different compounds, potassium hexabromoplatinate (K_2PtBr_6), potassium dicyanoaurate [$KAu(CN)_2$] and fluorescein mercuric acetate ($C_{24}H_{18}Hg_2O_9$), showed the potential for possible derivatives. About 5% of the data were collected as a heavy-atom survey for CPV crystals soaked in 1 m*M* K_2PtBr_6, 1 m*M* $KAu(CN)_2$ and 10 m*M* $C_{24}H_{18}Hg_2O_9$ for 12, 12 and 24 h, respectively. Since only a few films were obtained for each derivative [7 K_2PtBr_6 films, 9 $KAu(CN)_2$ films and 3 $C_{24}H_{18}Hg_2O_9$ films], there were not enough common or symmetry-related reflections for inter-film scaling. The scaling between films, within each derivative data set, was accomplished by using the native data as a reference. Post-refinement showed that the cell dimensions for the derivatives had decreased, with the biggest difference of 2·0 Å in the K_2PtBr_6 derivative, indicating a possible lack of isomorphism (Table 1). The lack of isomorphism was also revealed in the scaling of the native data set to each derivative data set, performed with mean local scaling in resolution and structure-factor amplitude ranges. Each of the derivative data sets exhibited large differences at both high and low resolution (Fig. 1).

Orientation of the virions in the crystal unit cell

A self-rotation function (Rossmann & Blow, 1962) was calculated using data between 50 and 12 Å resolution to search for twofold ($\kappa = 180°$), threefold ($\kappa = 120°$) and fivefold ($\kappa = 72$ or 144°) axes. About 14% of the largest terms were used to represent the second Patterson (Tollin & Rossmann, 1966). The

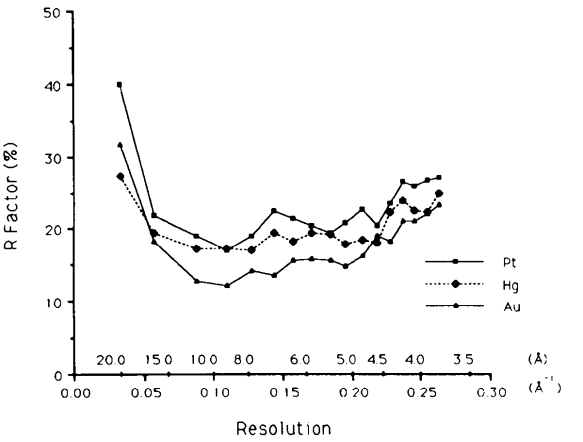

Fig. 1. *R* factor showing the difference between heavy-atom derivative and native amplitudes as a function of resolution. The increase of *R* factor at higher resolution (beyond 5.0 Å) suggests some lack of isomorphism. $R = (\sum||F_N| - k|F_{HN}||/\sum|F_N|) \times 100$, where F_N and F_{HN} are native and heavy-atom derivative structure amplitudes and k is a scale factor.

Table 1. *Data collection for the monoclinic crystal form*

(*a*) Data processed

	Native (full particles)	Native (empty particles)	K_2PtBr_6[a] (full particles)	$KAu(CN)_2$[b] (full particles)	$C_{24}H_{18}Hg_2O_9$[c] (full particles)
No. of films	253	47	7	9	3
R_{merge} (%)	12.2	15.5	15.3	15.1	11.67
$F^2 > n\sigma(F^2)$ where n =	2	3	2	2	2
No. of observed reflections	970 770	113 209	36649	40325	14809
No. of unique reflections	583 747	104 046	35089	39247	14667
Cell dimensions					
a (Å)	263.1		261.3	261.9	262.7
b (Å)	348.9		346.6	347.3	348.5
c (Å)	267.2		265.1	266.9	266.6
β (°)	90.8		90.9	90.9	90.8

(*b*) Percent of theoretically possible data in each resolution shell

Resolution shell (Å)	Native (full particles)	Native (empty particles)	K_2PtBr_6[a] (full particles)	$KAu(CN)_2$[b] (full particles)	$C_{24}H_{18}Hg_2O_9$[c] (full particles)
∞ -30	72	5	3	3	1
30-15	95	18	5	6	2
15-10	94	20	5	7	2
10-7.5	91	20	5	6	2
7.5-5.0	79	17	5	6	2
5.0-3.5	61	9	4	5	2
3.5-3.0	38	4	2	3	1
3.0-2.75	14	2	1	1	0

Derivatives are as follows: (*a*) K_2PtBr_6, potassium hexabromoplatinate; (*b*) $KAu(CN)_2$, potassium dicyanoaurate; (*c*) $C_{24}H_{18}Hg_2O_9$, fluorescein mercuric acetate.

radius of integration was set at 220 Å, which should have included most of the Patterson vectors generated within a virus particle. The interpolation grid around each rotated non-integral reciprocal lattice point was $3 \times 3 \times 3$. The function was explored in spherical polar coordinates in 1° intervals (Fig. 2). This established for the first time that parvoviruses do, indeed, possess near perfect icosahedral symmetry, in spite of the variability of their protein content. However, at 12 Å resolution only one set of broad peaks, corresponding to one set of icosahedral symmetry axes, could be observed, because one of the icosahedral twofold axes was, at least roughly, in the same direction as the crystallographic 2_1 axis.

When the self-rotation function was repeated, first for data between 12 and 7 Å and later with data between 5 and 4.3 Å resolution, each peak was split into two parts. This resulted in two sets of icosahedrally related peaks representing the two virus particles in the unit cell (Fig. 3). It was seen that there is a twofold axis inclined at 2.5° to the crystallographic b axis. The particle orientation was refined by an adaptation of the least-squares procedure of Rao & Rossmann (1973) to optimize the fit between the directions of the observed self-rotation function peaks from one of the virus particles and the corresponding axes of a standard icosahedron. The standard icosahedron is defined as shown in Fig. 3 with twofold axes along the orthogonal axes of the coordinate system. The position of each icosahedral symmetry axis in the standard setting is defined by the direction cosines (u',v',w'). The direction cosines for one of the CPV particles in the monoclinic cell are defined by the direction cosines u,v,w with respect to the orthogonal axes a^*, b, c such that

$$u = \sin\psi\cos\varphi$$
$$v = \cos\psi$$
$$w = -\sin\psi\sin\varphi$$

where ψ and φ are obtained from the rotation function and are the polar angles defining each symmetry axis (Rossmann & Blow, 1962). Then the matrix $[\rho]$ gives the rotation required to place the standard icosahedron on top of one of the particles in the monoclinic system such that

$$\begin{pmatrix} u \\ v \\ w \end{pmatrix} = [\rho] \begin{pmatrix} u' \\ v' \\ w' \end{pmatrix}.$$

It was found that

$$[\rho] = \begin{pmatrix} 0.5788 & 0.0111 & -0.8154 \\ 0.0304 & 0.9989 & 0.0352 \\ 0.8149 & -0.0452 & 0.5779 \end{pmatrix},$$

which implies that the standard icosahedron has to be rotated by $\kappa = -54.70°$ about an axis given by $\psi = 2.86°$ and $\varphi = 13.44°$ to correspond to one of the CPV particles in the crystal unit cell. The r.m.s. deviation between the directions of the observed

symmetry axes in the rotation function and those in the rotated standard icosahedron was 0.12 Å at a radius of 130 Å (which is about the largest radius of the CPV particle), corresponding to an angular error of 0.05°.

Position of the virions in the crystal unit cell

The rough position of the particles in the unit cell can be estimated by considering the packing of spheres into the $P2_1$ crystal cell (Luo *et al.*, 1988). To achieve the maximum separation of the two particle centers within the unit cell, it is necessary to place the particles at $(\frac{1}{4},Y,\frac{1}{4})$ and $(-\frac{1}{4},\frac{1}{2}+Y,-\frac{1}{4})$. This gives an average particle separation and, hence, diameter of 256 Å, comparable to electron microscopy observations (Tattersall & Gardiner, 1990; Tattersall & Cotmore, 1990).

A more accurate value was obtained by computing the Harker section of the Patterson function. As one of the noncrystallographic twofold axes was almost parallel to the crystallographic 2_1 axis, there will be a large Harker peak corresponding to the relative particle position in the unit cell. For a virion centered at (X,Y,Z), there is a crystallographically related virion at $(-X,\frac{1}{2}+Y,-Z)$. Similarly, for an atom at $(X+x,Y+y,Z+z)$, there will be another atom at $(-X-x,\frac{1}{2}+Y+y,-Z-z)$ as well as two additional atoms at $(X-x,Y+y,Z-z)$ and $(-X+x,\frac{1}{2}+Y+y,-Z+z)$ which are related by the icosahedral twofold axes parallel to b. Thus, there is a common vector $(2X,\frac{1}{2},2Z)$ between all atoms of one particle and its symmetry counterpart. When a Patterson was calculated with data between 30–15 Å resolution, a strong Harker peak was found at $(\frac{1}{2},\frac{1}{2},\frac{1}{2})$ (Fig. 4*a*). This confirmed that the particles were centered near $(\frac{1}{4},Y,\frac{1}{4})$. However, the peak became lower and elongated as the resolution of the data for the Patterson calculation was increased, and finally it split into two distinct peaks at 5 Å resolution (Fig. 4*b*), indicating that the particle center is slightly displaced from $(\frac{1}{4},Y,\frac{1}{4})$. The accuracy of such a particle center determination might be compromised by the inclination between the icosahedral twofold and monoclinic b axes. The starting position for phase refinement was selected from the R-factor search using an atomic model loosely based on the Mengo virus structure (Luo *et al.*, 1987). Confidence in this position was increased because it was within 1.5 Å of positions determined by other methods (Table 2). Some of these methods did not utilize the relationship between noncrystallographic and crystallo-

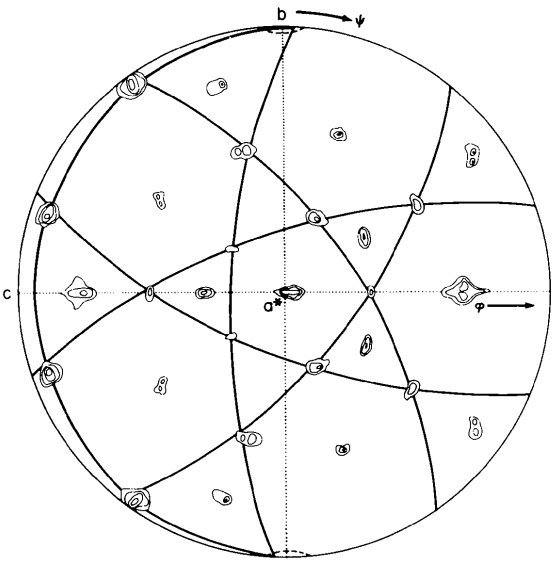

Fig. 2. Stereographic plot of CPV self-rotation function calculated between 50–12 Å resolution. At this resolution, the peaks of the two icosahedra are superimposed because one of the icosahedral twofold axes is roughly parallel to the crystallographic 2_1 axis. Sections at $\kappa = 180$, 120° and 72 or 144° have been combined into a single plot.

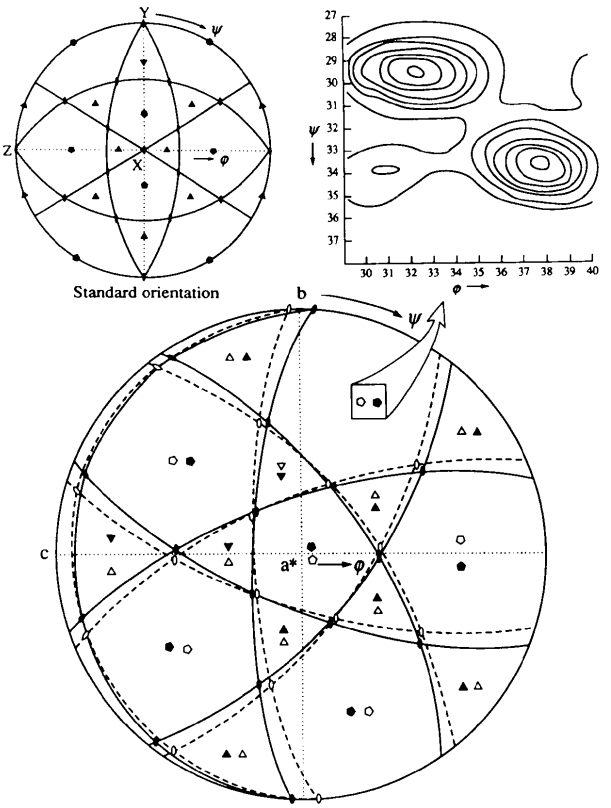

Fig. 3. High-resolution (to 4.3 Å) self-rotation function results showing the symmetry axes of two particles in the unit cell. Solid great circles connect the twofold axes for one icosahedron (with filled symmetry symbols) and the dashed great circles connect the other icosahedron (open symmetry symbols). The matrix $[\rho]$ (see text) rotates the standard icosahedron (inset) onto the observed self-rotation function peaks (connected with solid lines).

Table 2. *Determination of particle center*

Method	Resolution (Å)	X	Z	Displacement relative to final position (Å)
Harker section	5	0.2540	0.2420	1.34
Patterson projection	4	0.2521	0.2471	0.37
R-factor search with an atomic model	20	0.2544	0.2412	1.57
Fitting of spherical shells	13	0.2539	0.2382	2.35
Final refined position	3.8	0.2535	0.2470	

graphic symmetry, but are not prejudiced by the 2.5° inclination of the icosahedral axis to the monoclinic axis. Since all these methods gave answers within a radius of 1.4 Å, a satisfactory position appeared to have been determined for phase initiation at 20 Å resolution. The final refined particle position was fairly close to the highest peak in a noisy 4 Å resolution Patterson projection.

Initial phasing based on a hollow-shell model

Sets of initial phases were calculated from several hollow-shell models. 'Model-128', which was the most successful, had uniform density between an outer radius of 128 Å and an inner radius of 85 Å. The outer radius was consistent with the best packing of two spheres in the $P2_1$ unit cell and X-ray low-resolution scattering data (Chapman, Tsao & Rossmann, 1992: Schmidt, Johnson & Phillips, 1983). Structure factors were calculated for data between 150 and 20 Å resolution by Fourier back-transformation of the electron density. The phases were then used in conjunction with observed unweighted structure amplitudes for computation of an electron density map. This map was icosahedrally averaged within an envelope defined by an outer radius of 135 Å and an inner radius of 60 Å. Where there was overlap between particles, a tangential plane was chosen to separate them. The averaged map was again Fourier back-transformed to yield a new set of phases and cycling proceeded in the usual manner (Rossmann, 1990, and references therein). Ten cycles of averaging were performed at 20 Å resolution using only the weighted observed amplitudes and calculated phases. Ten additional cycles of averaging were calculated at 20 Å resolution in which the unobserved structure amplitudes were filled in with calculated structure factors. The phase extension to 11 Å then proceeded by increasing the resolution one reciprocal lattice unit at a time. Usually ten cycles of phase refinement followed each extension.

As the initial model consisted of spheres, the initial phases were constrained by a center of symmetry at (0,0,0). In general, such centricity should be removed by the first averaging cycle since a hand is arbitrarily chosen by the assignment of one or the other of the two icosahedral orientations to a selected particle position. However, if there had been no inclination of one of the icosahedral twofold axes to the crystallographic *b* axis, the phases would have remained centric. In the case of CPV, there was an icosahedral axis inclined by only 2.5° to the monoclinic axis. Extension of phases had to bridge the gap between low resolution, where a centric spherical model would be viable, and a resolution high enough such that the 2.5° inclination would be observable.

A comparison of phases extended from model-128 with those of two other models suggested that those

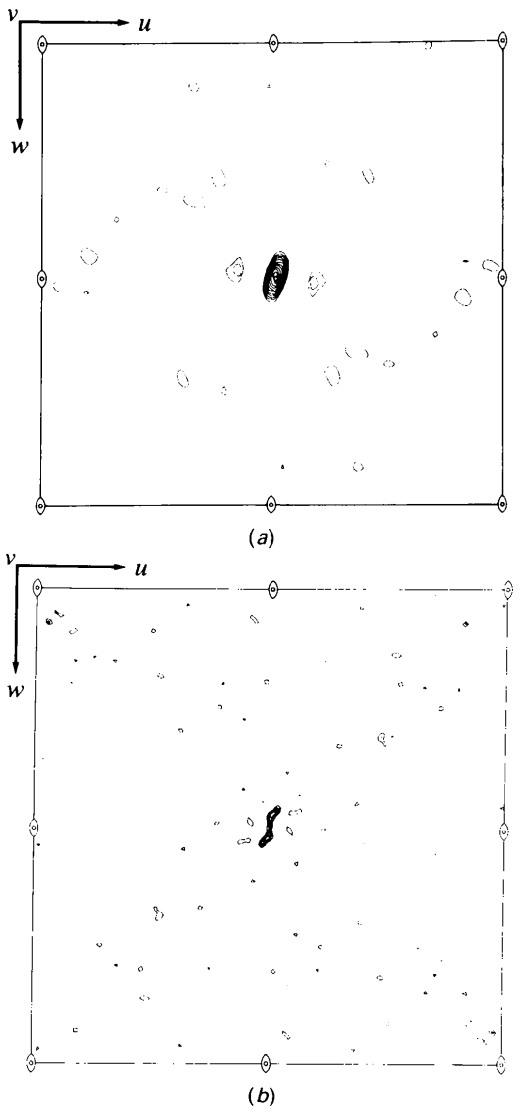

Fig. 4. Harker sections (*a*) at 15 Å and (*b*) at 5 Å resolution. The large peak at 15 Å resolution results from one of the noncrystallographic twofold axes being roughly parallel to the crystallographic 2_1 axis, and shows the particle center to be close to $(\frac{1}{4},Y,\frac{1}{4})$. At 5 Å resolution, the peak is split, indicating that the particle center is slightly displaced from $(\frac{1}{4},Y,\frac{1}{4})$.

of model-128 were basically correct. 'Model-122' and 'model-132' had outer radii of 122 and 131.7 Å and inner radii of 85 and 97 Å, respectively. They were based on fitting spherical shells to the low-resolution single-crystal X-ray data (Chapman *et al.*, 1992). At 20 Å resolution, the periodic Fourier transforms of these two models differed from each other by one node. The *R* factors and correlation coefficients at 13 Å resolution for the three different models are plotted in Fig. 5. The three phase sets were compared by examining the mean cosine phase difference as a function of resolution. A mean value of 1.0 would imply perfectly matching phases, a mean value of 0.0 would occur for randomly different phases and a mean of −1.0 would represent phases that are systematically shifted by 180°. The latter would correspond to an opposite Babinet solution with inverted electron density.

A comparison between phases determined from model-122 and phases determined from model-128 is shown in Fig. 6. The two sets of phases were reasonably correlated at less than 30 Å resolution, with a mean phase difference of 30°. However, the phases diverged at slightly higher resolution and were essentially uncorrelated at 20 Å resolution. Between 20 and 13 Å resolution, the cosine phase difference between model-122 and model-128 was negative, corresponding to a mean phase shift of 110°. That the correlation is negative implies that phases for Babinet opposite solutions have been selected, but as the correlation is imperfect there must be a mixture of both phase solutions, in opposition to each other. Therefore, although the two models agreed well at very low resolution, two opposite phase solutions (within the region where two sets have randomly correlated phases) had been 'fighting' each other, and when phases were extended beyond 20 Å resolution one solution dominated the other. A spherical shell is

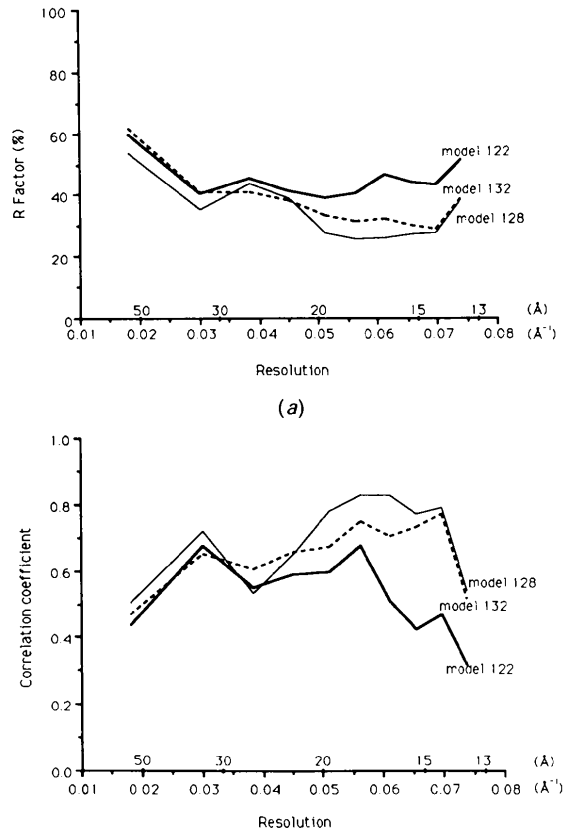

Fig. 5. The distribution of (*a*) *R* factors and (*b*) correlation coefficients for CPV phase extension from 20 to 13 Å resolution starting with three different hollow-shell models. Models-132, 128 and 122 have outer radii of 132, 128 and 122 Å, with inner radii of 97, 85 and 85 Å, respectively.

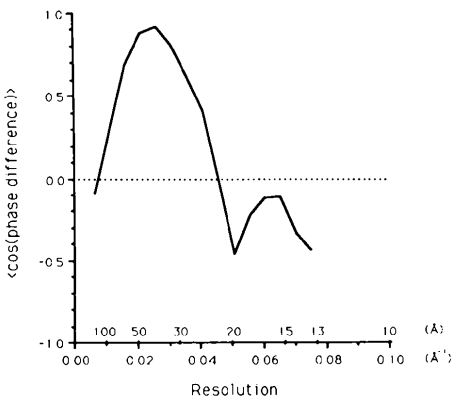

Fig. 6. Mean cosine phase difference between model-128 and model-122 following extension to 13 Å resolution.

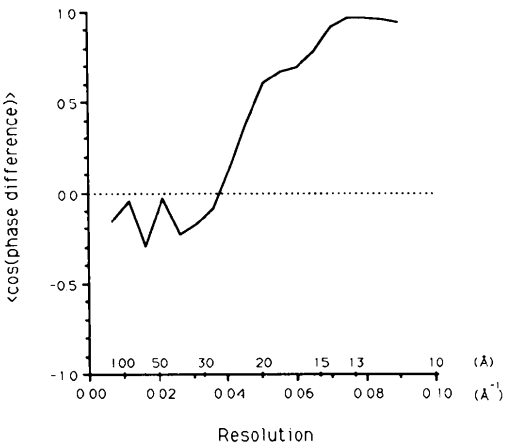

Fig. 7. Mean cosine phase difference between model-128 and model-132 following extension to 11 Å resolution. There is more or less random agreement between phases at resolution lower than 25 Å, phases were marginally correlated between 25–20 Å resolution, but the two phase sets gradually improved their agreement as phases were extended beyond 20 Å resolution. The mean phase difference between the two was less than 10° at 11 Å resolution.

an imprecise model for the CPV structure. Some of the initial calculated phases would be incorrect, being the Babinet opposite of the true phases. This would affect a larger proportion of the phases if the radii were incorrect, but it is likely that phases calculated from all models contained some Babinet opposites.

The phases (Fig. 7) and maps (Fig. 8) of model-128 and model-132 were compared after extension to 11 Å resolution. In spite of the difference in the outer radii, and hence in initial phases, by 11 Å resolution the phases and corresponding electron density maps were nearly identical. Electron density was mostly contained between an inner radius of 70 Å and an outer radius of 130 Å, differing from the radii of the initial models and the radii of the envelope used during the symmetry averaging and solvent flattening. These were good indications that the extended phases were tolerant of some errors in the initial model and were not biased towards the model or the molecular envelope, and, hence, might represent the correct solution.

Phases were then further extended to 9 Å resolution for model-128. However, the agreement between observed and calculated structure-factor amplitudes dropped steadily as resolution was increased and was not as good as that observed in the phase extension of other virus structure determinations started at higher (usually >8 Å) resolution (Luo *et al.*, 1987; Acharya *et al.*, 1989) (Fig. 9). Furthermore, the electron density distribution was not of sufficient resolution to judge whether the phases were likely to be right. This gave rise to some panic and doubt about the whole procedure. Later, after the structure was solved and the particle center had been refined, it was demonstrated that had a search been made, adjustment of the particle center would have been sufficient to carry the phase extension to high resolution (see *Concluding remarks*).

Isomorphous replacement

A survey was made of ten heavy-atom derivatives. A small amount of data was then collected for three of the most promising compounds (Table 1) for further assessment. The lack of isomorphism indicated by small cell-dimension changes (Table 1) and increased size of differences with resolution (Fig. 1) suggest that the derivatives were not promising.

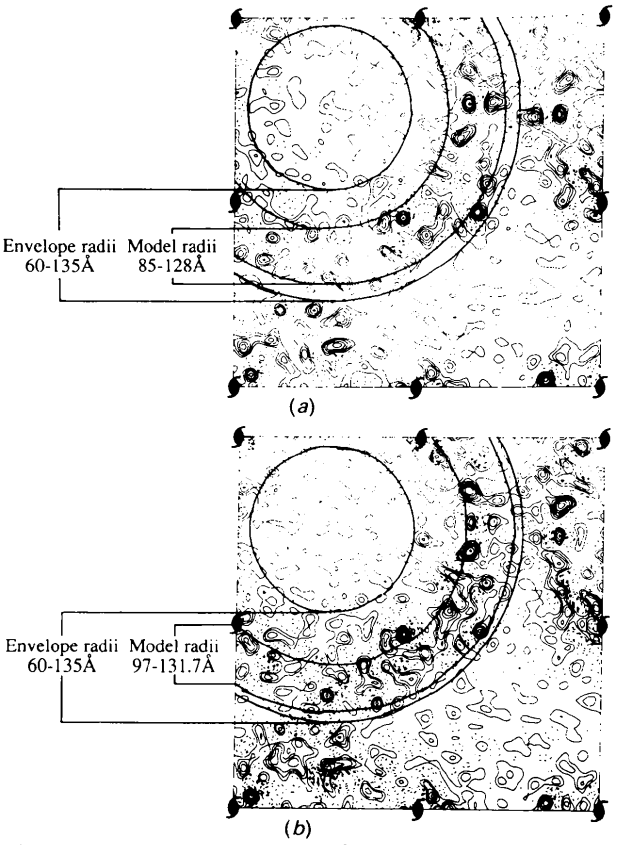

Fig. 8. Electron density maps at 11 Å resolution calculated using phases extended from (*a*) model-128 and (*b*) model-132.

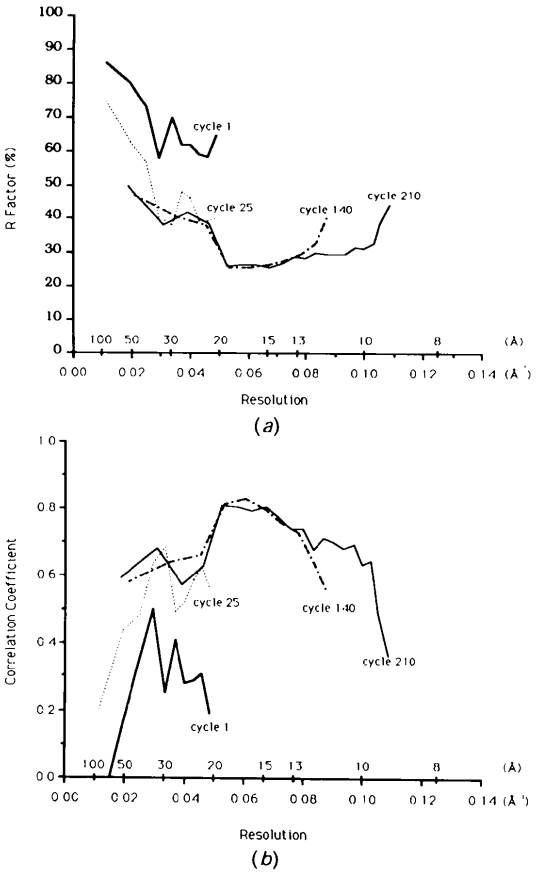

Fig. 9. (*a*), (*b*) Statistics of phase extension from 20 to 9 Å resolution starting from model-128.

Table 3. *Heavy-atom analysis*

(*a*) Heavy-atom parameters

Compound	Site	*x*	*y*	*z*	Occupancy on a relative scale	Relative to icosahedral axes (Å) *X*	*Y*	*Z*	Residue
K_2PtBr_6[a]	Pt1	0.1540	0.3703	0.1995	91	19.0	−19.5	129.0	Met87
$KAu(CN)_2$[b]	Au1	0.0950	0.2486	0.3435	26	52.3	0.0	85.0	Fivefold
$C_{24}H_{18}Hg_2O_9$[c]	Hg1	0.2708	0.2573	0.3075	60	8.8	18.5	89.0	Cys270
	Hg2	0.2852	0.2827	0.3001	62	4.8	19.3	98.0	Cys273

(*b*) Heavy-atom refinement analysis

Derivative		Resolution limits (Å) 15.6	10.4	7.8 Overall
K_2PtBr_6[a]	No. of reflections	754	619	1371
	R.m.s. lack of closure	65.8	61.3	
	Mean difference	89.9	83.7	
	f_H	57.4	56.8	
	Mean F_{VH}	16.6	17.1	
$KAu(CN)_2$[b]	No. of reflections	963	807	1770
	R.m.s. lack of closure	62.3	53.8	
	Mean difference	72.5	63.0	
	f_H	38.9	37.9	
	Mean F_{VH}	18.2	18.6	
$C_{24}H_{18}Hg_2O_9$[c]	No. of reflections	331	265	596
	R.m.s. lack of closure	59.6	57.7	
	Mean difference	81.2	85.6	
	f_H	52.1	59.1	
	Mean F_{VH}	16.2	16.1	

Derivatives are as follows: (*a*) K_2PtBr_6, potassium hexabromoplatinate; (*b*) $KAu(CN)_2$, potassium dicyanoaurate; (*c*) $C_{24}H_{18}Hg_2O_9$, fluorescein mercuric acetate.

Nevertheless, a difference Fourier synthesis was computed between the K_2PtBr_6 derivative and the native structure using data in the 15 to 9 Å resolution range. Phases used were those obtained from phase extension with model-128. The difference map was then 60-fold averaged and plotted with respect to orthogonal axes of the standard icosahedral setting (Fig. 10). The map density was mostly featureless except for a very large negative 'peak', with a magnitude more than twice that of any other peak (positive or negative). It was, therefore, immediately clear that a heavy-atom position had been located and that the phases represented the Babinet opposite solution of the structure. The Babinet inversion was caused by the inappropriate assumption of model radii.

The heavy-atom parameters, including the relative occupancy, temperature factor, position and scale factor, were adjusted by using a heavy-atom least-squares phasing and refinement program with non-crystallographic symmetry constraints (Rossmann, 1976) (Table 3). Knowledge of the heavy-atom site permitted refinement of the particle position. Since all the Pt sites within one virus particle were also related by icosahedral symmetry, the center of the particle lies at the center of gravity of these equivalent sites. The actual procedure used was to average the difference Fourier map at various positions near the previously determined particle center. A maximum in the heavy-atom peak led to a more accurate particle position (Fig. 11). The position of the Pt site within the asymmetric unit of the icosahedron was refined to $X = 19.0$, $Y = -19.5$ and $Z = 129$ Å, with respect to the standard orthogonal icosahedral axes, at a virus radius of 132 Å. Later, it was established that this site corresponded to Met87 on the viral surface.

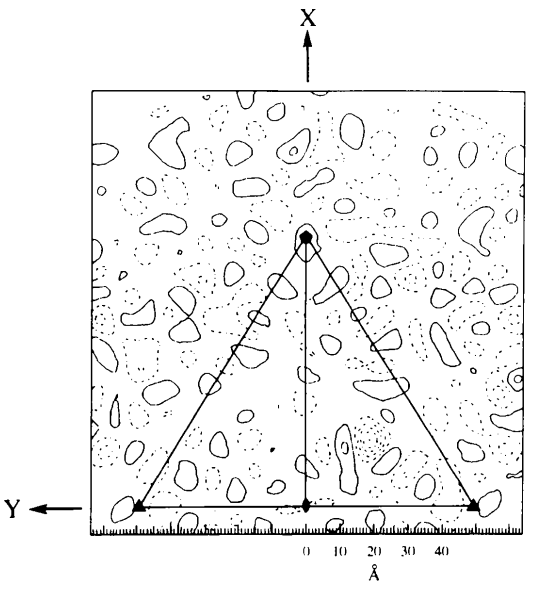

Fig. 10. A section ($Z = 129$ Å) of the skew averaged difference Fourier map calculated for the K_2PtBr_6 derivative using the phases extended to 9 Å resolution from the hollow-shell model-128. The large negative 'peak' corresponds to the Pt site.

Initial heavy-atom difference maps for the $C_{24}H_{18}Hg_2O_9$ and $KAu(CN)_2$ compounds did not give such obvious results, which was later attributed to lower substitution and lack of data. However, when final phases had been determined, these compounds were re-examined and found to occupy chemically reasonable sites (Table 3).

The SIR phases for the K_2PtBr_6 derivative were calculated to 8 Å resolution using the refined heavy-atom parameters and particle center. An electron density map based on SIR K_2PtBr_6 phases, representing 5% of the possible data, after 60-fold averaging in a large envelope, showed a shell of protein density (between radii of approximately 70–130 Å) in reasonable contrast to the solvent regions and the, presumably disordered, DNA core of the particle. One section of this map is shown in Fig. 12. This confirmed the correctness of the heavy-atom position and, in turn, further confirmed that the early phase solution was essentially correct, apart from the Babinet inversion.

Phase extension from the SIR phases

Molecular replacement phase refinement was re-initialized by using SIR phases between 15 and 8 Å resolution. The initial correlation coefficient was rather poor ($\simeq 0.2$), emphasizing the low quality of SIR phasing with a very partial data set. A radical improvement in the agreement between observed and calculated structure-factor amplitudes was observed after ten cycles of averaging. The correlation coefficient increased to 0.89 and the R factor dropped from 54.3 to 18.2% (Fig. 13).

The phases beyond 8 Å resolution were derived by phase extension in increments of one reciprocal lattice vector, with three to six cycles of phase refinement following each extension. The mean phase shift in the last cycle was usually about 5°. The molecular replacement phase extension then proceeded as previously described to 6 Å resolution. At this stage, an averaged electron density map showed clearly the density representing the secondary structure, mostly β-sheets, of a protein. The boundaries of the density led to a modified envelope with inner and outer envelope radii of 70 and 140 Å, respectively.

The position of the particle center was further refined as phase extension progressed (Fig. 14). This was done initially using the same approach as described above, by optimizing the height of the Pt peak in the difference map. This criterion failed

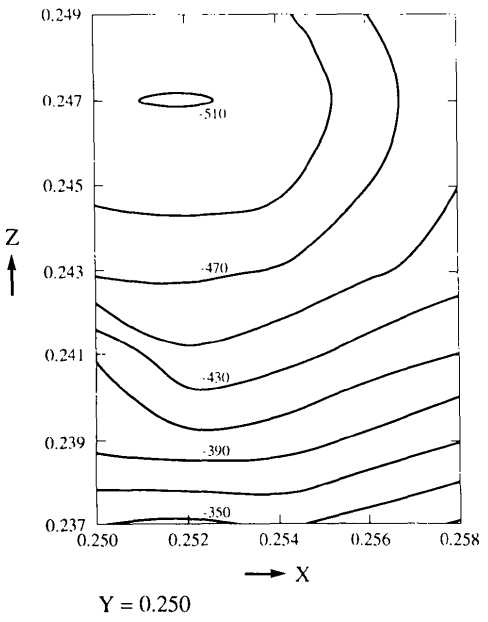

Fig. 11. The relative height of the Pt heavy-atom density plotted as a function of the position about which it was averaged.

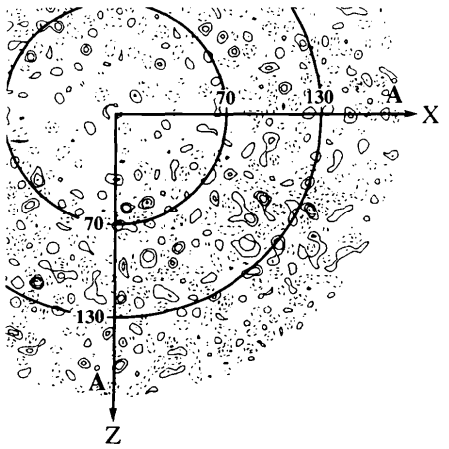

Fig. 12. Initial averaged electron density map calculated with SIR phases at 8 Å resolution showing a protein density shell between radii of 70 and 130 Å. The density outside a radius of 180 Å was set to zero during averaging.

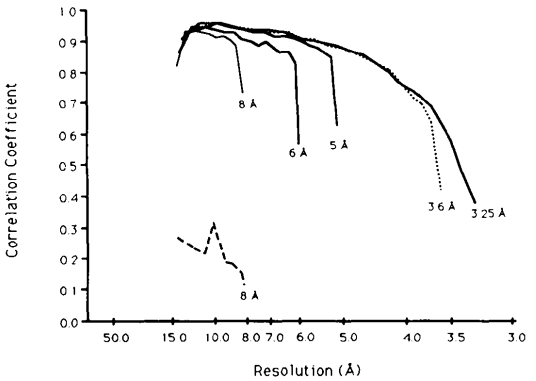

Fig. 13. Mean correlation coefficients during phase extension from the 8 Å resolution SIR phases to 3.25 Å resolution.

Table 4. *Refinement of particle position*

Technique	Refinement order	Resolution (Å)	Refined position x	Refined position z	Correlation coefficient Before	Correlation coefficient After
a	0	20.0	0.2544	0.2412		
b	1	9.0	0.2507	0.2473	0.68	0.84
b	2	6.0	0.2521	0.2464	0.88	0.91
c	3	5.5	0.2526	0.2466	0.88	0.91
c	4	5.1	0.2529	0.2468	0.89	0.91
c	5	4.0	0.2531	0.2469	0.88	0.89
c	6	3.8	0.2534	0.2470	0.87	0.89

Techniques used were as follows: (*a*) *R*-factor search with arbitrary atomic model; (*b*) maximizing averaged heavy-atom difference peak; (*c*) minimizing r.m.s. deviation of densities in the averaging procedure.

beyond 6 Å resolution due to the low quality of the derivative data and the lack of isomorphism at higher resolution. The refinement of the particle center was, therefore, switched to determine the location that gave the minimum r.m.s. deviation among the sets of 60 averaged electron densities (Table 4).

A total of 60 steps of phase extension were completed in extending phases from 8 Å resolution to 3.25 Å resolution (Fig. 13). The polypeptide chain tracing and amino-acid identification was completed on a 3.6 Å resolution 'mini' map, which had been skewed and averaged on a 1 Å grid and displayed with respect to the orthogonal axes of the standard icosahedron. Inspection of the β-sheets showed that the correct enantiomorph (for L-amino acids) would be obtained by making the transformation $\rho(X,Y,Z) = \rho(X,\overline{Y},Z)$.* Thus, the arbitrary selection of hand, made at the time of associating particle orientation with particle center, had been of the wrong absolute hand.

The polypeptide could be followed without any serious difficulty from one end to the other (except the first 37 residues which are disordered), and it was easy to associate the known sequence of CPV VP-2 with electron density. Bulky residues, for example Tyr-Tyr-Phe-Gln-Trp (residues 210–214), were recognized early (Fig. 15). The small side chains were also easily placed with considerable confidence. In addition, 11 sequential DNA nucleotides were recognizable, although the identity of the bases is uncertain. The detailed atomic model was built into a 3.25 Å electron density map using the interactive graphics program, *FRODO*, written by Alwyn Jones

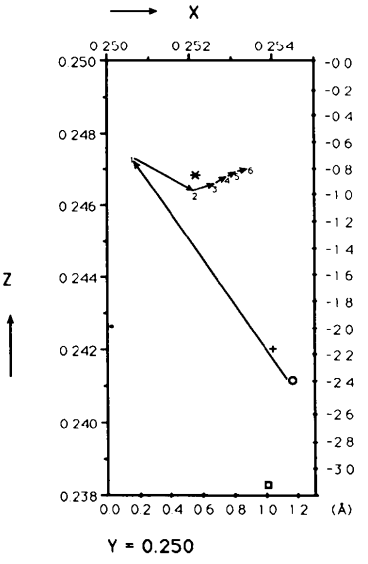

Fig. 14. The particle position was determined in several ways: by an *R*-factor search with an arbitrary atomic model (○) (the position used for initial phase extension), with a refinement procedure using a parameterized hollow-shell model (□), the Patterson projection at 4 Å resolution (*) and the Harker section at 5 Å resolution (+). Also shown are the steps (1, 2, ..., 6) in the refinement of the particle center as phasing progressed (Table 4).

* Let $\rho(\mathbf{X}') = \rho([T]\overline{\mathbf{X}})$ where $\mathbf{X}' = (X,\overline{Y},Z)$ and $\mathbf{X} = (X,Y,Z)$. Hence, to go from atomic coordinates (**X**) given in a right-handed system to fractional coordinates (**x**) in a right-handed system, it is necessary to apply the transformation $\mathbf{x} = [T^{-1}][\alpha][\rho][T]\mathbf{X}$ where $[\alpha]$ is the deorthogonalization matrix defined by Rossmann & Blow (1962) and $[\rho]$ is the rotation matrix defined earlier. Note, however, that the heavy-atom positions and particle center given in this manuscript were determined prior to the hand of the map. Hence, to convert these positions to a right-handed crystallographic coordinate system requires the transformation $\mathbf{x} = [T^{-1}][\alpha][\rho]\mathbf{X}$.

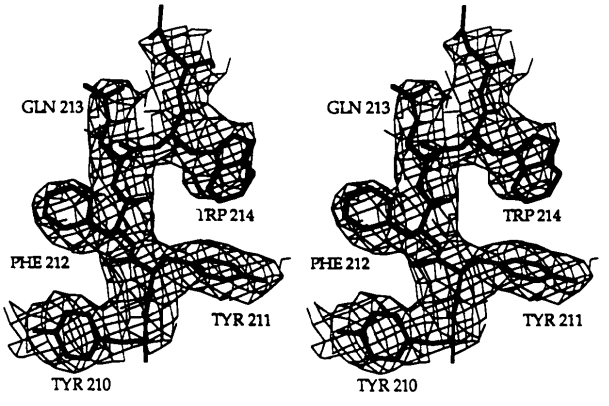

Fig. 15. Residues 210–214 (Tyr-Tyr-Phe-Gln-Trp) showing an example of the fit of the model to the electron density.

(Jones, 1978; Jones & Thirup, 1986). The polypeptide chain fold is shown in Fig. 16. This unrefined atomic structure gave an R factor of 36% for reflections between 5.0 and 3.25 Å resolution. The coordinates have been deposited with the Brookhaven Protein Data Bank.* A fuller discussion of the structure and its implications was given by Tsao *et al.* (1991).

Concluding remarks

Apart from the Babinet inversion, the phases obtained by extension from the hollow-shell model (model-128) were essentially correct. These phases, when compared to those extended from SIR, showed a mean cosine phase difference of -0.75 between 15 and 9 Å resolution, corresponding to a 41° mean error from the Babinet solution. The poor results of phases extended from model-128 to 9 Å resolution were probably caused by errors in the particle position (Fig. 17). To test this, the previously aborted extension of the model-128 phases was continued beyond 9 Å resolution without using SIR phase information, but having set the particle at its final refined position (Fig. 14, Table 4). Improvement in the agreement of observed and calculated structure-factor amplitudes was immediately observed. After three cycles of averaging, the correlation coefficient increased from 0.69 to 0.89 and the R factor dropped to 18.8%, comparable to that observed in the phase refinement of SIR phases (Fig. 18). The new phases were less than $180 \pm 10°$ from the final phases (Fig. 19). This result indicated that the CPV structure could have been solved without the use of SIR information, if the particle position had been accurately determined. It further demonstrated that phases for a spherical virus structure can be derived from a hollow spherical phasing model, provided all the important parameters (model radii, particle position and the diffraction data) are accurately determined.

We wish to thank Ming Luo for establishing the initial crystallization conditions; Greg Kamer and Sangsoo Kim for programming support; Mathur R. N. Murthy, Sangsoo Kim, Robert McKenna and Jin-bi Dai for help in data processing; Richard Compans and Sukla Basak for samples of CPV inoculant; many for help in synchrotron data collection (Jodi Bibler, S. Krishnaswamy, Robert McKenna, Andrew Prongay, Tom Smith, Liang Tong, Peter Willingmann and Di Xia); the staff of the CHESS, Daresbury, Brookhaven and DESY synchrotrons for their dedicated help; Kathy Smith for help with virus propagation; and, finally, Sharon Wilder for help in preparation of the manuscript. Fig. 15 was prepared by use of the programs *FRODO* (Jones, 1978) and *MACINPLOT* (Smith, 1990). WK was supported by a Schroedinger stipend

* Atomic coordinates and structure factors have been deposited with the Protein Data Bank, Brookhaven National Laboratory (Reference: 1DPV, R1DPVSF), and are available in machine-readable form from the Protein Data Bank at Brookhaven. The data have also been deposited with the British Library Document Supply Centre as Supplementary Publication No. SUP 37053 (as microfiche). Free copies may be obtained through The Technical Editor, International Union of Crystallography, 5 Abbey Square, Chester CH1 2HU, England.

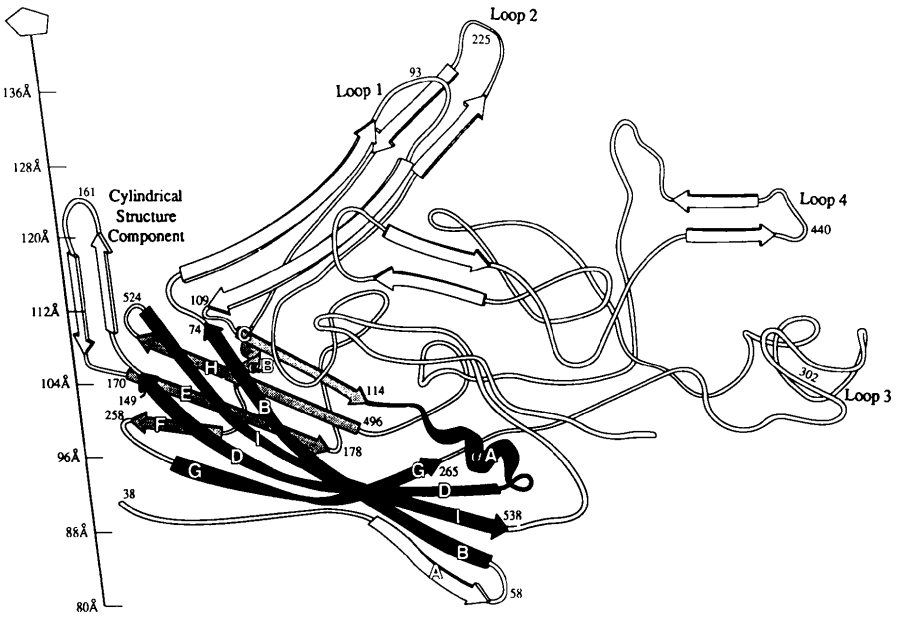

Fig. 16. Ribbon drawing of the VP-2 polypeptide topology. The β-sheet elements that correspond to equivalent structural elements in other viruses are labeled βB, βC, ..., βI and are darker. Large insertions between the β-strands of the eight-stranded antiparallel β-barrel are grey. Four loops, which together with equivalent structure from two other threefold related subunits make up threefold 'spikes', are labeled loops 1, 2, 3 and 4. Amino-acid sequence numbers are given in strategic places. The approximate radial distance from the viral center in Å is shown along the fivefold axis. [Reprinted with permission from Tsao *et al.* (1991). © American Association for the Advancement of Science.]

from the Austrian Science Foundation and HW by a predoctoral fellowship from the Howard Hughes Medical Institute. The work was supported by grants to MGR from the National Institutes of Health and the National Science Foundation and by a Markey Foundation grant supporting the expansion of structural studies at Purdue University.

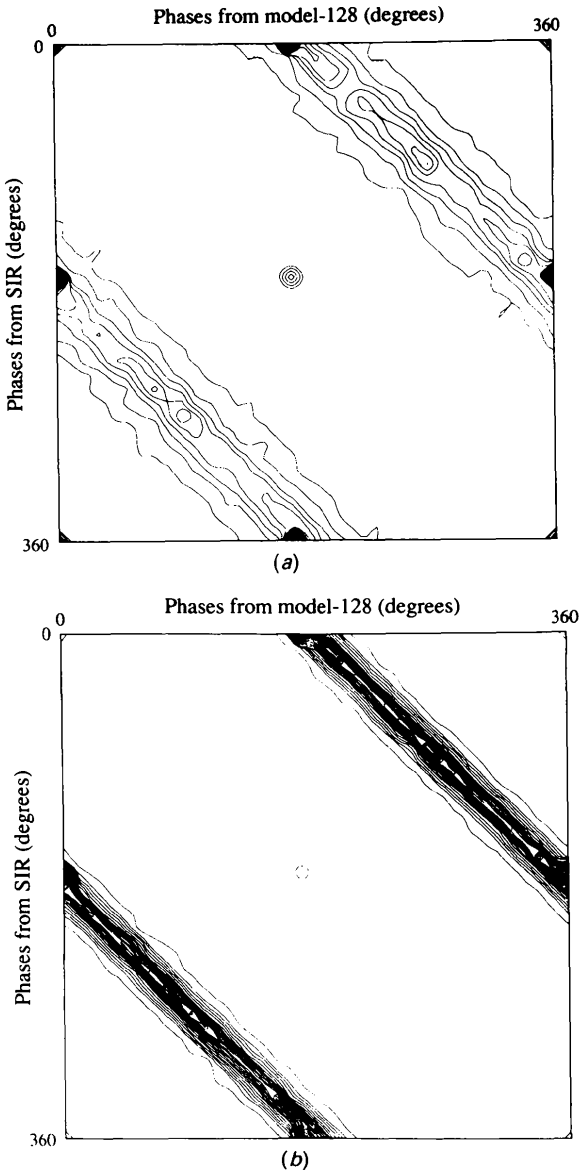

Fig. 17. Comparison of phases refined from SIR with those derived from model-128 (*a*) when placed at the initial position and (*b*) when placed at the final refined position. The plots show the frequency with which a phase of one set corresponds to a phase of the other. The dominance along the line $\alpha_1 = \alpha_2 + 180°$ indicates that the model-derived phases had a Babinet opposite solution to those of the refined SIR phases. The larger scatter in (*a*) is caused by the small error in the position of the particle center used for averaging the electron density.

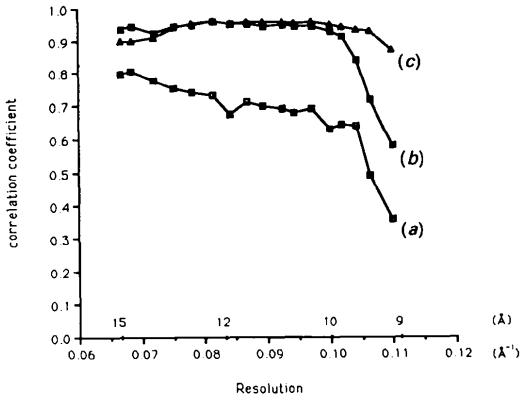

Fig. 18. Refinement of phases obtained from model-128 (*a*) with the particle at the original position, (*b*) after setting the particle to the final refined position, and (*c*) the correlation coefficients between 15 and 9 Å resolution for the actual structure determination.

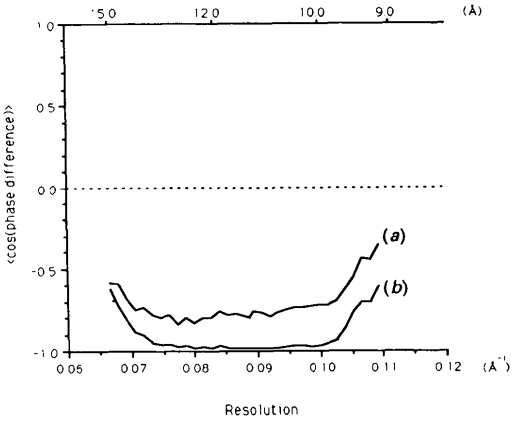

Fig. 19. Mean cosine phase difference between the final CPV phases and those extended from the hollow-shell model using (*a*) the initial and (*b*) the refined particle position.

References

ACHARYA, R., FRY, E., STUART, D., FOX, G., ROWLANDS, D. & BROWN, F. (1989). *Nature (London)*, **337**, 709–716.

CHAPMAN, M. S., TSAO, J. & ROSSMANN, M. G. (1992). *Acta Cryst.* A**48**. In the press.

HOGLE, J. M., CHOW, M. & FILMAN, D. J. (1985). *Science*, **229**, 1358–1365.

HOSUR, M. V., SCHMIDT, T., TUCKER, R. C., JOHNSON, J. E., GALLAGHER, T. M., SELLING, B. H. & RUECKERT, R. R. (1987). *Proteins*, **2**, 167–176.

JOHNSON, J. E., AKIMOTO, T., SUCK, D., RAYMENT, I. & ROSSMANN, M. G. (1976). *Virology*, **75**, 394–400.

JONES, T. A. (1978). *J. Appl. Cryst.* **11**, 268–272.

JONES, T. A. & THIRUP, S. (1986). *EMBO J.* **5**, 819–822.

KIM, S. (1989). *J. Appl. Cryst.* **22**, 53–60.

KIM, S., SMITH, T. J., CHAPMAN, M. S., ROSSMANN, M. G., PEVEAR, D. C., DUTKO, F. J., FELOCK, P. J., DIANA, G. D. & MCKINLAY, M. A. (1989). *J. Mol. Biol.* **210**, 91–111.

KURTZMAN, G., FRICKHOFEN, N., KIMBALL, J., JENKINS, D. W., NIENHUIS, A. W. & YOUNG, N. S. (1989). *N. Engl. J. Med.* **321**, 519–523.

LUO, M., TSAO, J., ROSSMANN, M. G., BASAK, S. & COMPANS, R. W. (1988). *J. Mol. Biol.* **200**, 209–211.

LUO, M., VRIEND, G., KAMER, G., MINOR, I., ARNOLD, E., ROSSMANN, M. G., BOEGE, U., SCRABA, D. G., DUKE, G. M. & PALMENBERG, A. C. (1987). *Science*, **235**, 182–191.
PARADISO, P. R. (1981). *J. Virol.* **39**, 800–807.
PARADISO, P. R., RHODE, S. L. & SINGER, I. I. (1982). *J. Gen. Virol.* **62**, 113–126.
PARRISH, C. R., HAVE, P., FOREYT, W. J., EVERMANN, J. F., SENDA, M. & CARMICHAEL, L. E. (1988). *J. Gen. Virol.* **69**, 1111–1116.
RAO, S. T. & ROSSMANN, M. G. (1973). *J. Mol. Biol.* **76**, 241–256.
RAYMENT, I., BAKER, T. S., CASPAR, D. L. D. & MURAKAMI, W. T. (1982). *Nature (London)*, **295**, 110–115.
ROSSMANN, M. G. (1976). *Acta Cryst.* A**32**, 774–777.
ROSSMANN, M. G. (1979). *J. Appl. Cryst.* **12**, 225–238.
ROSSMANN, M. G. (1990). *Acta Cryst.* A**46**, 73–82.
ROSSMANN, M. G., ARNOLD, E., ERICKSON, J. W., FRANKENBERGER, E. A., GRIFFITH, J. P., HECHT, H. J., JOHNSON, J. E., KAMER, G., LUO, M., MOSSER, A. G., RUECKERT, R. R., SHERRY, B. & VRIEND, G. (1985). *Nature (London)*, **317**, 145–153.
ROSSMANN, M. G. & BLOW, D. M. (1962). *Acta Cryst.* **15**, 24–31.
ROSSMANN, M. G., LESLIE, A. G. W., ABDEL-MEGUID, S. S. & TSUKIHARA, T. (1979). *J. Appl. Cryst.* **12**, 570–581.
SCHMIDT, T., JOHNSON, J. E. & PHILLIPS, W. E. (1983). *Virology*, **127**, 65–73.
SMITH, T. J. (1990). *J. Appl. Cryst.* **23**, 141–142.
STUDDERT, M. J. (1990). *CRC Handbook of Parvoviruses*, Vol. II, edited by P. TIJSSEN, pp. 3–27. Boca Raton: CRC Press.
TATTERSALL, P. & COTMORE, S. F. (1990). *CRC Handbook of Parvoviruses*, Vol. I, edited by P. TIJSSEN, pp. 123–140. Boca Raton: CRC Press.
TATTERSALL, P. & GARDINER, E. M. (1990). *CRC Handbook of Parvoviruses*, Vol. I, edited by P. TIJSSEN, pp. 111–121. Boca Raton: CRC Press.
TOLLIN, P. & ROSSMANN, M. G. (1966). *Acta Cryst.* **21**, 872–876.
TSAO, J., CHAPMAN, M. S., AGBANDJE, M., KELLER, W., SMITH, K., WU, H., LUO, M., SMITH, T. J., ROSSMANN, M. G., COMPANS, R. W. & PARRISH, C. R. (1991). *Science*, **251**, 1456–1464.

Acta Cryst. (1992). B**48**, 88–95

Comparison of the Structures of the Enantiomeric and Racemic Forms of an Imidazo[2,1-*b*]thiazole Anthelmintic Agent and their Hydrochlorides

BY KÁLMÁN SIMON

Chinoin Pharmaceutical and Chemical Works Co. Ltd, Research Center, POB 110, *H*-1325 *Budapest, Hungary*

MÁRIA ÁCS

Department of Organic Chemical Technology, Technical University of Budapest, POB 91, *H*-1521 *Budapest, Hungary*

SINE LARSEN

Department of Physical Chemistry, The H. C. Ørsted Institute, University of Copenhagen, Universitetsparken 5, *DK*-2100 *Copenhagen Ø, Denmark*

AND VILMOS FÜLÖP AND ESZTER GÁCS-BAITZ

Central Research Institute for Chemistry of the Hungarian Academy of Sciences, POB 17, *H*-1525 *Budapest, Hungary*

(*Received* 17 *April* 1991; *accepted* 2 *August* 1991)

Abstract

Structure determinations were performed on 6-phenyl-2,3,5,6-tetrahydroimidazo[2,1-*b*]thiazole bases and their hydrochloride salts. The structures of the optically active base (LEVA), two polymorphic racemic bases (TETRA and TETRA2) and the racemic hydrochloride (TETRA.HCl) are compared both with each other and with the known structure of the optically active hydrochloride (LEVA.HCl) [Baker & Pauling (1973). *J. Chem. Soc. Perkin Trans.* 2, pp. 203–206]. LEVA, TETRA and TETRA2: $C_{11}H_{12}N_2S$, $M_r = 204.3$. LEVA: orthorhombic, $P2_12_12_1$, $a = 4.851$ (1), $b = 9.746$ (1), $c = 21.864$ (1) Å, $V = 1033.6$ Å^3, $D_x = 1.31$ g cm^{-3}, $Z = 4$, λ(Cu $K\alpha$) = 1.5418 Å, $\mu = 23.97$ cm^{-1}, $F(000) = 432$, $T = 296$ K, $R = 0.033$ for 1168 reflections [$I > 3.0\sigma(I)$]. TETRA: monoclinic, $P2_1/n$, $a = 9.557$ (1), $b = 9.773$ (1), $c = 11.286$ (1) Å, $\beta = 105.6$ (3)°, $V = 1015.3$ Å^3, $D_x = 1.336$ g cm^{-3}, $Z = 4$, λ(Cu $K\alpha$) = 1.5418 Å, $\mu = 24.40$ cm^{-1}, $F(000) = 432$, $T = 296$ K, $R = 0.053$ for 1962 reflections [$I > 3.0\sigma(I)$].

0108-7681/92/010088-08$03.00